Research Square

Preprints are preliminary reports that have not undergone peer review.
They should not be considered conclusive, used to inform clinical practice,
or referenced by the media as validated information.

Features of Second-Harmonic Generation of Femtosecond Laser Pulses in a β-BaB_2O_4 (BBO) Crystal

Bogibek Gayrat ugli Urinov
Urgench State University named after Abu Rayhan Biruni
Atabek Salievich Ashirov
Urgench State University named after Abu Rayhan Biruni
Shuhrat Baxtiyar ugli Shamuratov
Mamun University
Erkaboy Yusubovich Davletov
Mamun University
Obid Ikrambayevich Sabirov
sabirov.o@mamunedu.uz

Mamun University
Alisher Erkaboy ugli Rajabov
Mamun University
Usman Kalandarovich Sapaev
Mamun University

Research Article

Keywords:

Posted Date: November 12th, 2026

DOI: https://doi.org/10.21203/rs.3.rs-11510864/v1

License: This work is licensed under a Creative Commons Attribution 4.0 International License.
Read Full License

Additional Declarations: No competing interests reported.

Features of Second-Harmonic Generation of Femtosecond Laser Pulses in a β-BaB_2O_4 (BBO) Crystal

B.G. Urinov[1], A.S. Ashirov[1], Sh.B. Shamuratov[2], E.Y. Davletov[2], O.I. Sabirov[2*], A.E. Rajabov[2], U.K. Sapaev[2]

[1]Department of Electrical Engineering and Energy, Urgench State University named after Abu Rayhan Biruni, 14 Kh. Alimdjan Str., Urgench, 220100, Uzbekistan.

[2*]Mamun University, Sanoatchilar str. 9, Urgench, Khorezm Region, 220100, Uzbekistan.

*Corresponding author(s). E-mail(s): sabirov.o@mamunedu.uz;

Abstract

In this work, second-harmonic generation (SHG) of femtosecond laser pulses in a $\boldsymbol{\beta}$-$\mathbf{BaB_2O_4}$ (BBO) nonlinear crystal is analyzed theoretically. To describe the spatiotemporal dynamics of the fundamental and second-harmonic pulses, a system of coupled-wave equations accounting for group-velocity dispersion (GVD), third-order dispersion (TOD), and group-velocity mismatch (GVM) is employed. The equations are solved numerically using the split-step Fourier method combined with a fourth-order Runge–Kutta algorithm. For fundamental radiation at $\boldsymbol{\lambda_1 = 1658.6}$ nm, the type-I ($\boldsymbol{oo \rightarrow e}$) phase-matching angle $\boldsymbol{\theta_{pm} \approx 19.95^\circ}$ and the effective nonlinear coefficient $\boldsymbol{d_{\text{eff}} \approx 2.12}$ pm/V are obtained. Simulation results are presented for pulse durations of $\boldsymbol{\tau = 10}$, 200, 500, and 1000 fs. In addition, the growth of SHG efficiency with crystal length is analyzed, together with the trade-off between the pump intensity required to achieve a given efficiency and the sensitivity to dispersion. The results provide practical guidelines for selecting the crystal length and pulse duration in the design of BBO-based femtosecond frequency converters.

Keywords: second-harmonic generation, $\boldsymbol{\beta}$-$\mathbf{BaB_2O_4}$ (BBO), phase matching, femtosecond laser pulses, group-velocity dispersion, group-velocity mismatch, nonlinear optics, split-step Fourier method, Runge–Kutta method

1 Introduction

Second-harmonic generation (SHG) is one of the fundamental processes of nonlinear optics, in which two photons at frequency ω are coherently converted into a single photon at frequency 2ω. This process extends the spectral range of laser sources into the visible and ultraviolet regions, where direct laser emission is often limited or entirely unavailable. The SHG efficiency is governed by two interrelated factors: the magnitude of the second-order nonlinear susceptibility $\chi^{(2)}$ of the medium and the fulfilment of the phase-matching condition $\Delta k = k_{2\omega} - 2k_{\omega} = 0$. When this condition is satisfied, energy is transferred continuously from the fundamental wave to the second harmonic; otherwise, it oscillates periodically between the two waves [1].

Among second-order nonlinear crystals, β-BaB_2O_4 (BBO) occupies a special place. It is transparent over a wide wavelength range (approximately 190–3500 nm) and can therefore be used in the ultraviolet, visible, and infrared regions. BBO is highly resistant to intense laser radiation, i.e., it has a high laser-induced damage threshold. Owing to the large difference between the refractive indices of the ordinary and extraordinary waves ($\Delta n = n_o - n_e$), phase matching can be achieved over a broad spectral range by choosing the angle between the wave vector and the optic axis. Furthermore, BBO possesses a relatively large nonlinear coefficient ($d_{\text{eff}} \approx 2.2$ pm/V) and very low linear absorption.

BBO is a negative uniaxial crystal whose ordinary and extraordinary refractive indices are described with high accuracy as functions of wavelength by Sellmeier equations. Recent studies have shown that cascaded processes in BBO can generate high-order harmonics of 800 nm laser radiation, yielding vacuum-ultraviolet radiation down to 133 nm. This also enables reliable calculation of phase-matching parameters, namely the phase-matching angle and the spectral and angular acceptance bandwidths [2]. Owing to these properties, BBO crystals are widely used for deep-ultraviolet generation [3, 4], in tunable coherent sources in the far-ultraviolet region, for second-harmonic generation at 266 nm in waveguides [4, 5], and for high-order harmonic generation driven by two-color laser fields.

In the femtosecond regime, the nature of the SHG process changes considerably. As the pulse duration decreases, its spectral bandwidth increases. Consequently, the phase-matching condition ($\Delta k = 0$) is exactly satisfied only at the central frequency, whereas for the other spectral components of the pulse the phase mismatch $\Delta k(\omega)$ is nonzero. Moreover, the fundamental and second-harmonic pulses propagate in the crystal with different group velocities. This group-velocity mismatch (GVM) causes the pulses to walk off from each other in time and shortens the distance over which they can interact. Group-velocity dispersion (GVD) and third-order dispersion (TOD), in turn, modify the temporal shape and duration of the pulses. For this reason, classical results obtained in the monochromatic approximation, including the theoretical analysis of phase-mismatched SHG in BBO, cannot fully describe the femtosecond regime [6, 7].

In [7], the spatiotemporal dynamics of SHG of ultrashort pulses in BBO was investigated; the authors interpreted the process as a combination of simultaneous SHG and sum-frequency generation through multiple spectral channels. In [8], highly efficient SHG of chirped femtosecond pulses in BBO was analyzed, and it was shown that long crystals make it possible to achieve high conversion efficiency even at low pump

intensity, but at the cost of a sharp increase in the sensitivity of SHG to pulse dispersion. To address the problem of broadband phase matching, approaches such as the use of angularly dispersed beams have also been proposed [9, 10].

The aim of this work is to theoretically investigate second-harmonic generation of femtosecond pulses with a fundamental wavelength of 1658.6 nm in a BBO crystal under type-I ($oo \rightarrow e$) phase matching, taking into account group-velocity dispersion (GVD), third-order dispersion (TOD), and group-velocity mismatch (GVM). To this end, the phase-matching angle and the effective nonlinear coefficient were determined, and the coupled-wave equations were solved numerically using the split-step Fourier method and the fourth-order Runge–Kutta method. In addition, the influence of pulse duration (τ = 10, 200, 500, and 1000 fs) on the conversion dynamics was analyzed, the dependence of the conversion efficiency on crystal length was studied, and the optimal balance between the required pump intensity and the sensitivity to dispersion was evaluated.

2 Theoretical Model and Numerical Methods

2.1 Nonlinear polarization and the phase-matching condition

In a noncentrosymmetric medium, the second-order nonlinear polarization induced by a strong optical field is expressed as [11, 12]:

$$P^{(2)}(2\omega) = \varepsilon_0 \chi^{(2)} E^2(\omega), \tag{1}$$

where ε_0 is the vacuum permittivity, $E(\omega)$ is the complex amplitude of the fundamental electric field, and $\chi^{(2)}$ is the second-order nonlinear susceptibility tensor of the medium. Efficient energy transfer from the fundamental wave to the second harmonic requires the phase-matching condition to be satisfied:

$$\Delta k = k_{2\omega} - 2k_{\omega} = 0, \tag{2}$$

where k_{ω} and $k_{2\omega}$ are the wave vectors of the fundamental and second-harmonic waves, respectively. In dispersive media such as BBO, this condition is usually satisfied only for a particular combination of propagation direction (θ, φ) and wavelength, i.e., by angular (birefringent) phase matching.

2.2 Type-I ($oo \rightarrow e$) phase matching in BBO

BBO is a negative uniaxial crystal, in which the refractive index of the ordinary wave exceeds that of the extraordinary wave ($n_o > n_e$). In this work, type-I ($oo \rightarrow e$) phase matching between the fundamental and second-harmonic waves is considered. The refractive indices are calculated using the Sellmeier equations of Kato (1986) [12, 13]:

$$n_o^2(\lambda) = 2.7359 + \frac{0.01878}{\lambda^2 - 0.01822} - 0.01354\lambda^2, \tag{3}$$

$$n_e^2(\lambda) = 2.3753 + \frac{0.01224}{\lambda^2 - 0.01667} - 0.01516\lambda^2, \tag{4}$$

where λ is the wavelength in micrometers. The effective refractive index of an extraordinary wave propagating at an angle θ to the optic axis is given by

$$\frac{1}{n_e^2(\theta)} = \frac{\cos^2\theta}{n_o^2} + \frac{\sin^2\theta}{n_e^2}. \tag{5}$$

The type-I phase-matching angle θ_{pm} is determined from the condition $n_o(\omega) = n_e(2\omega, \theta_{pm})$. The values calculated for the fundamental wavelength $\lambda_1 = 1658.6$ nm (corresponding to the second-harmonic wavelength $\lambda_2 = 829.3$ nm) are listed in Table 1.

Table 1 Calculated phase-matching parameters of BBO for the fundamental wavelength $\lambda_1 = 1658.6$ nm (type I, $oo \rightarrow e$).

Parameter	Symbol	Value
Phase-matching angle	θ_{pm}	19.95°
Ordinary refractive index (pump)	$n_o(\lambda_1)$	1.6448
Extraordinary refractive index (SH)	$n_e(\lambda_2, \theta_{pm})$	1.6448
Phase mismatch (at the central frequency)	Δk	≈ 0 (exact phase matching)
Effective nonlinear coefficient	d_{eff}	2.12 pm/V

2.3 Coupled-wave equations including dispersion

The spatiotemporal dynamics of SHG in the femtosecond regime is described by a system of coupled-wave equations for the slowly varying envelopes of the fundamental and second-harmonic fields. In contrast to the continuous-wave or picosecond regimes, femtosecond pulse propagation requires explicit inclusion of dispersive effects.

The evolution equations for the complex field envelopes $A_1(z,t)$ and $A_2(z,t)$ are

$$\begin{aligned}
&\frac{\partial A_1}{\partial z} + \frac{1}{v_{g1}}\frac{\partial A_1}{\partial t} - \frac{ik_1''}{2}\frac{\partial^2 A_1}{\partial t^2} + \frac{\alpha_1}{2}A_1 = -i\frac{\omega_1}{2n_1 c}\chi^{(2)} A_1^* A_2\, e^{i\Delta k z}, \\
&\frac{\partial A_2}{\partial z} + \frac{1}{v_{g2}}\frac{\partial A_2}{\partial t} - \frac{ik_2''}{2}\frac{\partial^2 A_2}{\partial t^2} + \frac{\alpha_2}{2}A_2 = -i\frac{\omega_2}{2n_2 c}\chi^{(2)} A_1^2\, e^{-i\Delta k z},
\end{aligned} \tag{6}$$

where v_{g1} and v_{g2} are the group velocities of the fundamental and second-harmonic waves, k_1'' and k_2'' are the corresponding group-velocity dispersion (GVD) coefficients, α_1 and α_2 are the linear absorption coefficients, n_1 and n_2 are the refractive indices, and c is the speed of light in vacuum.

The second-order temporal derivatives account for pulse broadening and temporal distortion induced by GVD, while the first-order temporal derivatives describe the group-velocity mismatch (GVM) between the interacting waves. The model therefore captures both temporal walk-off and dispersive pulse deformation, which are critical in the femtosecond regime [13].

Equation (6) is solved by the split-step Fourier method. At each step dz, the dispersive (linear) part is first evaluated over a half-step $dz/2$ in the Fourier domain by multiplication with a phase factor. The nonlinear coupling is then integrated over the full step dz using the fourth-order Runge–Kutta method. Finally, the dispersive part is evaluated again over a half-step $dz/2$. This approach is consistent with the numerical methods used in [14] and [15].

2.4 Initial conditions and numerical parameters

The fundamental pulse incident on the crystal is assumed to be a Fourier-transform-limited (chirp-free) Gaussian pulse:

$$\begin{cases} A_1(z=0,t) = A_0 \exp\left[-2\ln 2\left(\dfrac{t}{\tau}\right)^2\right], \\ A_2(z=0,t) = \eta_{\text{seed}} A_0, \end{cases} \tag{7}$$

where A_0 is the peak amplitude of the pulse and τ is the pulse duration defined as the full width at half maximum (FWHM) of the intensity. The second-harmonic field at the crystal input is assumed to be negligibly small (seed level η_{seed}).

The main parameters used in the simulations are listed in Table 2.

Table 2 Main parameters used in the numerical simulations.

Parameter	Value
Fundamental wavelength, λ_1	1658.6 nm
Second-harmonic wavelength, λ_2	829.3 nm
Peak intensity, I_1	1 GW/cm^2 (10^{13} W/m^2)
Pulse duration, τ	10–1000 fs (variable)
Time grid, $N \times \Delta t$	4096×0.1 fs
Propagation step, Δz	5 μm
Numerical method	Split-step Fourier + RK4 (fourth order)

3 Results and Discussion

3.1 Effect of pulse duration on the conversion dynamics

Figure 1 shows the second-harmonic conversion efficiency η as a function of the propagation distance z in the crystal for four pulse durations ($\tau = 10$, 200, 500, and 1000 fs). The conversion process clearly depends strongly on the pulse duration. For the shortest pulse ($\tau = 10$ fs), the efficiency increases slowly and smoothly, and high values are reached only at $z \approx 0.3$ cm. This is because the spectrum of such a short pulse is very broad ($\sim$400 nm), whereas phase matching is satisfied only near the central frequency, so the other spectral components are poorly converted to the second harmonic. In

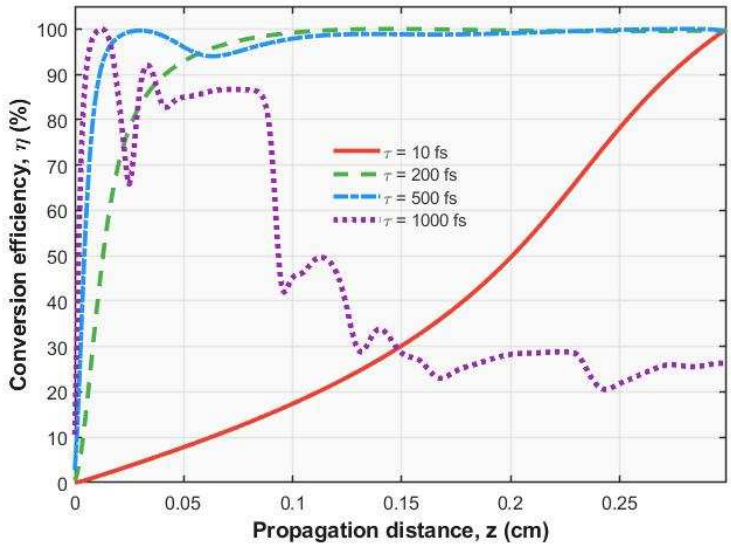


Fig. 1 Second-harmonic conversion efficiency η as a function of crystal length z for different pulse durations: $\tau = 10$ fs (red), 200 fs (green, dashed), 500 fs (blue, dash-dotted), and 1000 fs (purple, dotted).

addition, the fundamental and second-harmonic pulses propagate with different velocities and quickly separate from each other. For $\tau = 200$ fs, the efficiency increases rapidly and, beyond $z \approx 0.1$ cm, saturates at a level close to $\sim$100%. In this case, the pulse spectrum fits within the phase-matching bandwidth and temporal walk-off has almost no effect on the process; no back-conversion is observed. For $\tau = 500$ fs, the efficiency reaches $\sim$99% over a very short distance ($z \approx 0.03$ cm), followed by a slight decrease and recovery. This is a consequence of weak back-conversion: part of the second-harmonic energy is transferred back to the fundamental wave. Finally, for the longest pulse ($\tau = 1000$ fs), the maximum efficiency is reached at the shortest distance ($z \approx 0.01$ cm), after which the efficiency oscillates strongly and decreases to $\sim$25–45%. This behavior is associated with repeated energy exchange between the fundamental and second-harmonic waves, i.e., strong back-conversion.

Each pulse duration thus has its own optimal crystal length. For long pulses ($\tau \geq 500$ fs), short crystals (≤ 0.03 cm) are sufficient, whereas in longer crystals the efficiency decreases due to back-conversion. For $\tau \approx 200$ fs, the efficiency is least sensitive to the crystal length, which is the most favorable case from a practical standpoint. For very short pulses ($\tau \approx 10$ fs), high efficiency is achieved only in longer crystals, but at the cost of pulse-shape distortion.

Figure 2 shows the dependence of the second-harmonic conversion efficiency on the BBO crystal length for pulses with duration $\tau = 50$ fs and intensity $I_1 = 1$ GW/cm^2. The efficiency increases with crystal length, but the growth is not uniform: the curve has an S-shaped form with three distinct regions. In the first region ($L < 1.5$ mm), the efficiency increases slowly and amounts to only $\sim$2.5% at $L = 1$ mm. Here the second

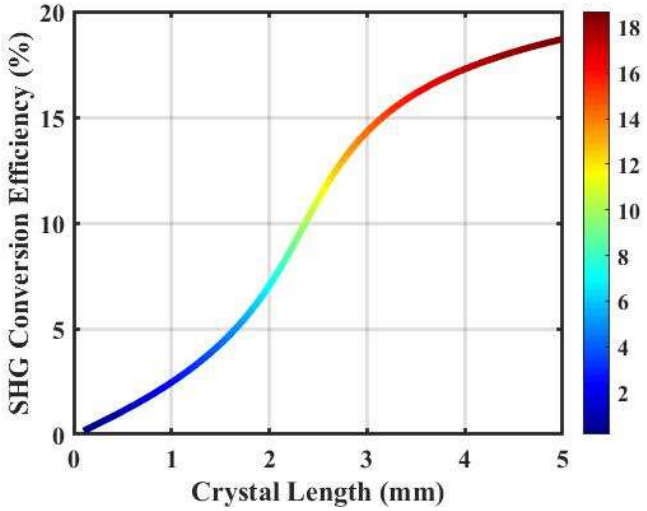


Fig. 2 Second-harmonic conversion efficiency in a BBO crystal as a function of crystal length L ($\lambda_1 = 1658.6$ nm, $\tau = 50$ fs, $I_1 = 1$ GW/cm^2, type-I $oo \to e$ interaction).

harmonic is only beginning to build up, and the fundamental energy is practically undepleted; the efficiency grows in proportion to the square of the crystal length. In the second region (1.5–3 mm), the efficiency grows most rapidly, reaching ∼14% at $L = 3$ mm. The inflection point of the curve, where the growth rate is maximal, is located near $L \approx 2.2$ mm. This is the most effective part of the crystal: the fundamental and second-harmonic pulses still overlap as they propagate, and the second harmonic is continuously amplified. In the third region ($L > 3$ mm), the growth of efficiency slows down, reaching ∼18.7% at $L = 5$ mm. Since the efficiency is still low, this slowdown is not caused by depletion of the fundamental wave; rather, it results from dispersion effects inherent to femtosecond pulses.

First, the fundamental and second-harmonic pulses propagate in the crystal with different group velocities (GVM). The longer the crystal, the more they separate, and the weaker their interaction becomes.

Second, owing to dispersion (GVD), the pulse broadens in time. As a result, its peak intensity decreases and the second harmonic builds up more slowly.

Third, the spectrum of a 50 fs pulse is broad (∼80 nm), and phase matching is fully satisfied only at the central frequency, whereas the spectral wings are poorly converted to the second harmonic. This effect becomes stronger as the crystal length increases.

Thus, increasing the crystal length from 1 mm to 3 mm raises the efficiency by a factor of approximately 5.5, whereas increasing it from 3 mm to 5 mm adds only ∼4.5 percentage points, while the output pulse becomes more distorted by dispersion. Therefore, under the conditions considered, the optimal crystal length is estimated to be $L \approx 3$ mm. To further increase the efficiency, it is preferable to raise the pump intensity rather than lengthen the crystal, provided that the intensity remains below the laser-induced damage threshold of BBO.

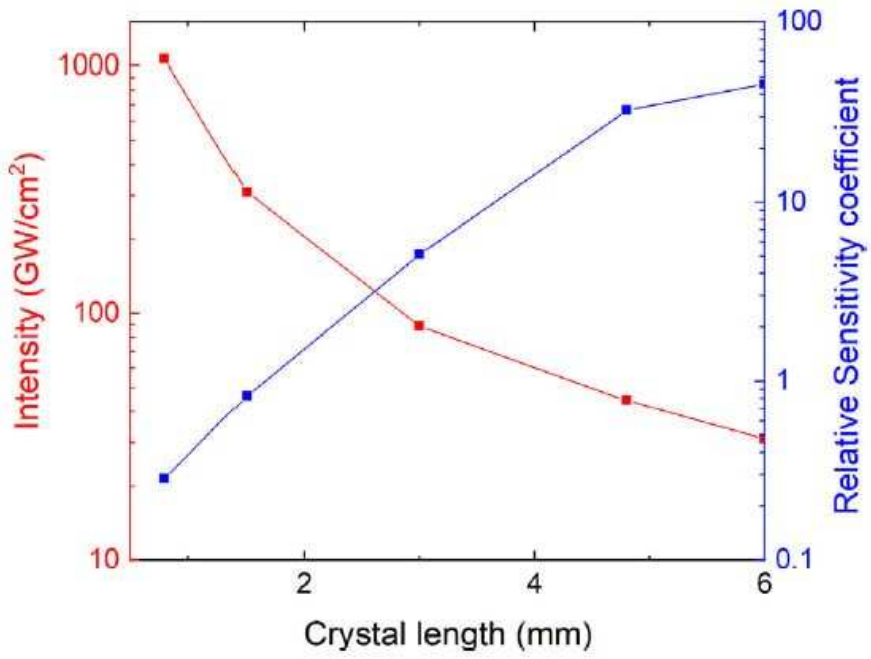


Fig. 3 Effect of the nonlinear crystal length L ($0.75 \leq L \leq 6$ mm) on two key parameters: the radiation intensity I (GW/cm^2) required to drive the nonlinear process and the relative sensitivity coefficient S of the system. Both quantities are plotted on a logarithmic scale.

The results show that the required intensity decreases monotonically with increasing crystal length: from $I \approx 1.0{\times}10^3$ GW/cm^2 at $L \approx 0.75$ mm to $I \approx 3{\times}10^1$ GW/cm^2 at $L = 6$ mm. Thus, an eightfold increase in the nonlinear interaction length reduces the intensity threshold by a factor of approximately 30–35. This dependence is approximated by a power law of the form $I \propto L^{-n}$ ($n \approx 1.7$–2). This result agrees with the theoretically expected behavior of second-order nonlinear processes: in the approximation of perfect phase matching and an undepleted pump, the conversion efficiency is given by $\eta \propto d_{\text{eff}}^2\, I\, L^2$. Hence, maintaining the same efficiency requires $I \propto L^{-2}$. The steeper decrease in intensity at small L (0.75–3 mm) and the flattening of the curve at large L indicate the presence of additional limiting factors.

The relative sensitivity coefficient exhibits the opposite behavior: as the crystal length increases, S grows from ≈ 0.3 to ≈ 45, i.e., by approximately two orders of magnitude. In the range 0.75–4.8 mm, the $S(L)$ dependence is nearly linear in semi-logarithmic coordinates, indicating a rapid growth of sensitivity. In the range 4.8–6 mm, the growth rate slows considerably (from $S \approx 32$ to $S \approx 45$), which may be attributed to a transition to a saturation regime. Possible reasons for this behavior include the narrowing of the phase-matching bandwidth in inverse proportion to L, the temporal separation of the interacting waves due to their group-velocity mismatch, and the spatial walk-off of the beams.

The two curves intersect at $L \approx 2.6$–2.8 mm. This region represents the balance point between reducing the required intensity and maintaining an acceptable level of system sensitivity.

Thus, the results confirm that crystal length is a decisive factor in optimizing the parameters of a nonlinear optical system. Increasing the crystal length significantly lowers the required intensity threshold, thereby reducing the risk of laser-induced optical damage to the crystal. However, this comes at the cost of a sharp increase in the sensitivity of the system to variations in external parameters (angle of incidence, temperature, spectral bandwidth). Consequently, the choice of crystal length should be based on a compromise between a low intensity requirement and high stability. According to the analysis, crystal lengths in the range of 3–5 mm are optimal for the system considered, since in this range the intensity threshold is below 10^2 GW/cm^2, while the sensitivity remains at a manageable level before the onset of saturation.

4 Conclusions

In this work, second-harmonic generation of femtosecond laser pulses in a β-BaB_2O_4 (BBO) nonlinear crystal was investigated using a comprehensive numerical model (split-step Fourier + RK4) that simultaneously accounts for group-velocity dispersion, third-order dispersion, and group-velocity mismatch. For the fundamental wavelength $\lambda_1 = 1658.6$ nm, the type-I ($oo \to e$) phase-matching angle $\theta_{pm} \approx 19.95^\circ$ and the effective nonlinear coefficient $d_{\text{eff}} \approx 2.12$ pm/V were determined.

The study of the influence of pulse duration showed that the relationship between the group-velocity walk-off length L_{GVM} and the transform-limited spectral bandwidth determines the qualitative character of the conversion dynamics: for ultrashort pulses ($\tau = 10$ fs), the broad spectrum smooths out periodic back-conversion oscillations, resulting in monotonic growth, whereas for long pulses ($\tau = 1000$ fs), the narrow spectrum brings the process close to the quasi-monochromatic regime, giving rise to deep periodic back-conversion oscillations.

The analysis of the crystal-length dependence showed that the growth curve of conversion efficiency follows an approximately quadratic law at small lengths and begins to saturate around $L \approx L_{\text{GVM}}(\tau)$, which confirms the internal consistency between the two independent numerical experiments (varying the pulse duration and varying the crystal length). Finally, the analysis of the trade-off between the required pump intensity and the sensitivity to dispersion showed that BBO follows the general trend observed in other nonlinear crystals such as LBO (short crystal: high stability but high intensity requirement; long crystal: low intensity requirement but low stability).

The results are of practical importance for the design of compact BBO-based femtosecond frequency converters: when selecting the optimal crystal length, one should take into account not only the maximum conversion efficiency but also the pulse duration, the optical damage threshold, and the robustness of the system with respect to its dispersion settings. Future studies may focus on applying broadband phase-matching techniques to BBO, such as angularly dispersed schemes and quasi-phase-matched structures.

References

[1] Abdul Rahman, M., Alghoraibi, I.: Theoretical investigation of phase-mismatched second-harmonic conversion efficiency in BBO crystal. Optik **161**, 196–203 (2018) https://doi.org/10.1016/j.ijleo.2018.01.126

[2] Seres, J., Seres, E., Schumm, T.: Cascaded multi-harmonic generation in a β-BBO crystal reaching 133 nm from a single 800 nm pump beam. Preprint, Technische Universität Wien (2025)

[3] Devi, K., Parsa, S., Ebrahim-Zadeh, M.: Birefringent-multicrystal, single-pass, continuous-wave second-harmonic-generation in deep-ultraviolet. In: Proc. SPIE, vol. 9894, p. 98940 (2016). https://doi.org/10.1117/12.2227630

[4] Miyazaki, K., Sakai, H., Sato, T.: Efficient deep-ultraviolet generation by frequency doubling in β-BaB_2O_4 crystals. Optics Letters **11**(12), 797–799 (1986) https://doi.org/10.1364/OL.11.000797

[5] Bhar, G.C., Chatterjee, U., Rudra, A.M., Kumbhakar, P.: Tunable coherent far-UV generation by frequency conversion in BBO. Quantum Electronics **29**(9), 800–805 (1999)

[6] Akhmedov, M., Sadullayev, J., Vapayev, M., Tojinazarov, F., Davletov, I., Rayimbaev, J.: Effects of picosecond pulsed laser radiation on crater formation on copper foil surfaces. Engineering Research Express **8**(3), 035401 (2026) https://doi.org/10.1088/2631-8695/ae3b9d

[7] Hong, L.-H., Chen, B.-Q., Hu, C.-Y., Li, Z.-Y.: Spatial–temporal evolution of ultrashort laser pulse second harmonic generation in β-barium borate (β-BBO) crystal. Journal of Applied Physics **129**, 233102 (2021) https://doi.org/10.1063/5.0052422

[8] Dansette, P.M., Burokas, R., Veselis, L., Zaukevičius, A., Michailovas, A., Rusteika, N.: Peculiarities of second harmonic generation with chirped femtosecond pulses at high conversion efficiency. Optics Communications **455**, 124462 (2020) https://doi.org/10.1016/j.optcom.2019.124462

[9] Akhmedov, M., Sadullayev, J., Vapayev, M., Matnazarov, A., Davletov, I., Rayimbaev, J.: Picosecond-pulsed laser ablation of aluminum foils: crater morphology and plasma parameters. Engineering Research Express **7**(3), 035362 (2025) https://doi.org/10.1088/2631-8695/ae0092

[10] Rajabov, A.E., Sabirov, O.I., Urinov, B., Assanto, G., Sapaev, U.K.: On high-efficiency third-harmonic generation via cascaded $\chi^{(2)}$ processes in orientation-patterned GaAs. Photonics **13**(8), 717 (2026) https://doi.org/10.3390/photonics13080717

[11] Sabirov, O.I., Akbarova, N., Atadjanova, N., Sapaev, U.K.: Efficient realization of infrared coherent radiation by the method of parametric light amplification in nonlinear photonic crystals. Journal of Physics: Conference Series **2131**(5), 052092 (2021) https://doi.org/10.1088/1742-6596/2131/5/052092

[12] Shi, M., Zhang, G., Li, B., Li, R., Yan, T., Luo, M., Ye, N.: Efficient frequency conversion for cubic harmonic generation at 266 nm in centrosymmetric α-BBO crystal. Optics Letters **43**(8), 1734–1737 (2018) https://doi.org/10.1364/OL.43.001734

[13] Sabirov, O.I., Ashirov, A.S., Sapaev, U.K.: Numerical analysis of femtosecond second-harmonic generation in periodically poled GaN crystals. Journal of Russian Laser Research **47**(3), 240–249 (2026)

[14] Sabirov, O.I., Rajabov, A.E., Matnazarov, A.R., Eshchanov, B.K., Otajanov, S., Sapaev, U.K.: Study of femtosecond laser amplification in MgO:$LiTaO_3$ crystals with periodic non-linear properties. Nanosystems: Physics, Chemistry, Mathematics **16**(3), 291–297 (2025) https://doi.org/10.17586/2220-8054-2025-16-3-291-297

[15] Arisholm, G., Biegert, J., Schlup, P., Hauri, C.P., Keller, U.: Ultra-broadband chirped-pulse optical parametric amplifier with angularly dispersed beams. Optics Express **12**(3), 518–530 (2004) https://doi.org/10.1364/OPEX.12.000518